Showcasing research from Professor Vicky Montiel-Palma's laboratory, Department of Chemistry, Mississippi State University, Starkville, United States of America.

Unexpected alkyl isomerization at the silicon ligand of an unsaturated Rh complex: combined experiment and theory

The equilibrium established between a monomer and its dimer is a fundamental process in biochemical and chemical transformations. Also fundamental is the isomerization of alkyl metal complexes. Yet, isomerization of an alkyl ligand substituent is exceptional and must involve migration of the substituent to the metal. Herein, we show that silyl substituents on a phosphinosilyl ligand at Rh can be isomerized from isopropyl to *n*-propyl during the metalation of $[RhCl(COD)]_2$ and the silylphosphine. A common intermediate was computationally identified to give rise to a Rh monomeric complex or its corresponding isomerized dimer. The change of only one *n*-propyl group is enough to favor dimer formation!

Artwork by Gaby Sanchez-Lecuona.

As featured in:

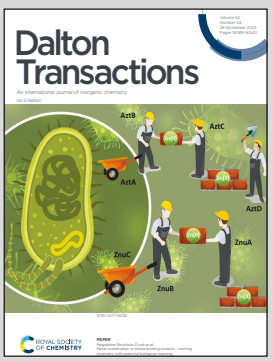

See Charles Edwin Webster, Virginia Montiel-Palma *et al.*, *Dalton Trans.*, 2023, **52**, 16159.

ROYAL SOCIETY OF CHEMISTRY

rsc.li/dalton

Registered charity number: 207890

Dalton Transactions

ROYAL SOCIETY OF CHEMISTRY

PAPER

Check for updates

Cite this: *Dalton Trans.*, 2023, **52**, 16159

Unexpected alkyl isomerization at the silicon ligand of an unsaturated Rh complex: combined experiment and theory†

Niroshani S. Abeynayake,‡ Nghia Le,‡ Gabriela Sanchez-Lecuona, Bruno Donnadieu, Charles Edwin Webster * and Virginia Montiel-Palma *

Received 3rd July 2023,
Accepted 8th October 2023

DOI: 10.1039/d3dt02087h

rsc.li/dalton

The formation of dimer [(μ-Cl)Rh-(κ^3(*P*,*Si*,*Si*)PhP(*o*-$C_6H_4CH_2Si^iPr_2$)(*o*-$C_6H_4CH_2Si^iPr^nPr$))]$_2$ (**Rh-3**) with an *n*-propyl group on one of the silicon atoms as a minor product was affected by the reaction of [RhCl(COD)]$_2$ with proligand PhP(*o*-$C_6H_4CH_2SiH^iPr_2)_2$, **L1**. The major product of the reaction was monomeric 14-electron Rh(III) complex [ClRh(κ^3(*P*,*Si*,*Si*)PhP(*o*-$C_6H_4CH_2Si^iPr_2)_2$)] (**Rh-1**). Computations revealed that the monomer–dimer equilibrium is shifted toward the monomer with four isopropyl substituents on the two Si atoms of the ligand as in **Rh-1**; conversely, the dimer is favored with only one *n*-propyl as in **Rh-3**, and with less bulky alkyl substituents such as in [ClRh(κ^3(*P*,*Si*,*Si*)PhP(*o*-$C_6H_4CH_2SiMe_2)_2$]$_2$ (**Rh-2**). Computations on the mechanism of formation of **Rh-3** directly from [RhCl(COD)]$_2$ are in agreement with the experimental findings and it is found to be less energetic than if stemming from **Rh-1**. Additionally, a Si–O–Si complex, [μ-Cl-Rh{κ^3(*P*,*Si*,*C*)PPh(*o*-$C_6H_4CH_2Si^iPrO\ Si^iPr_2CH$-*o*-$C_6H_4$)}]$_2$, **Rh-4**, is generated from the reaction of **Rh-1** with adventitious water as a result of intramolecular C–H activation.

Introduction

The equilibrium established between a monomer and its corresponding dimer is a fundamental process involved in crucial steps in biochemical and chemical transformations. From mitochondrial,[1] DNA[2] and enzymatic functions[3] to the proliferation of cancer cells,[4–6] and the mechanisms involved in diseases such as Parkinson,[7] malaria,[8] and others,[9] monomer–dimer equilibria are invoked. In transition metal catalysis, dissociative processes of dimeric complexes to unsaturated intermediates are often postulated as yielding catalytically active species. Often, the mechanisms of catalysis of Rh dimer complexes implicate the formation of 14-electron monomers.[10,11] Some examples include the hydroformylation of terminal alkenes with formaldehyde;[12] the carbonylative coupling of iodobenzenes with furfural;[13] the enantioselective Suzuki–Miyaura cross-coupling of racemic substrates;[14] and the coupling of terminal alkynes with carboxylic acids,[15,16] amongst others.

Our group reported a family of Ir(III) and Rh(III) complexes derived from a semirigid arylphosphine substituted with two di-isopropylsilane groups, [PhP(*o*-$C_6H_4CH_2Si^iPr_2H)_2$] (**L-1**, Scheme 1), as selective catalysts for the dehydrogenative silylation or hydrosilylation of styrenes and internal alkenes.[17]

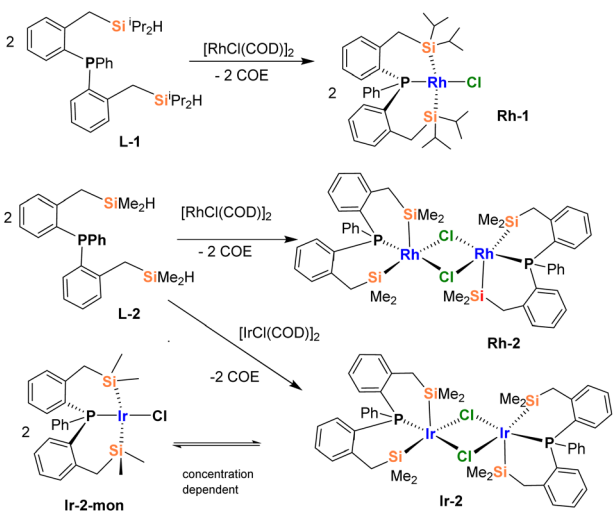

Scheme 1 The synthesis of Rh and Ir(III) complexes bearing methyl or isopropyl substituted (κ^3-*Si*,*Si*,*P*) silylphosphine ligands.

Department of Chemistry, Mississippi State University, Box 9573, Mississippi State, Mississippi 39762, USA. E-mail: ewebster@chemistry.msstate.edu, vmontiel@chemistry.msstate.edu

† Electronic supplementary information (ESI) available: Full experimental details of the synthesis of all compounds including the NMR spectra and X-ray diffraction data of complexes **Rh-3** and **Rh-4**. CCDC 2133159 and 2133161. For ESI and crystallographic data in CIF or other electronic format see DOI: https://doi.org/10.1039/d3dt02087h

‡ These authors contributed equally to this work.

Stable monomeric 14 electron complexes [X-M(κ^3(*P*,*Si*,*Si*)PhP(*o*-$C_6H_4CH_2Si^iPr_2)_2$)] (M = Ir, X = Cl (**Ir-1**), Me;[19] M = Rh, X = Cl (**Rh-1**, Scheme 1),[18] Br, I, OTf, Cl·$GaCl_3$)[17] stemmed from the reactions of [$MCl(COD)_2$] in arenic (benzene, toluene), ethereal (THF, Et_2O) and/or chlorinated solvents (chloroform, dichloromethane) displaying saw-horse geometries around the metal center. We found no evidence of stabilizing agostic interactions.[17] Each silicon atom arranges *trans* to a vacant coordination site, evidencing high stabilization by its strong *trans* influence, a consequence of its strong σ-donating nature.[20–22] The analogous di-methyl substituted proligand [PhP(*o*-$C_6H_4CH_2SiMe_2H)_2$] (**L-2**, Scheme 1) gives rise to dinuclear 16-electron complexes [(μ-Cl)M(κ^3(*P*,*Si*,*Si*)PhP(*o*-$C_6H_4CH_2SiMe_2)_2$)]$_2$ (M = Rh, **Rh-2**; Ir, **Ir-2**),[23,24] where the metals achieve a square pyramidal geometry with a Si atom occupying an axial site, *trans* to a vacant coordination site.

Herein, we report the isolation of **Rh-3** (Scheme 2), a complex derived from ligand **L-1**, in which a single isopropyl substituent per coordinated ligand undergoes isomerization to *n*-propyl. The isomerized complex is found as a dimer in contrast to the monomeric nature of **Rh-1**. DFT computations of the monomer–dimer equilibrium show that it is indeed shifted to the monomer in **Rh-1** and to the dimer in **Rh-3** (Scheme 3). The computed values for ΔH and ΔG demonstrate the more favorable nature of dimer **Rh-3** bearing one *n*-propyl substituent on Si per ligand, in comparison with the **Rh-1-dimer** with all isopropyl substituents. The present work exemplifies a consequence of the relatively rare reversible Si–C(sp^3) bond activation previously observed in pincer PSiP motifs,[25–29] in our case giving rise to alkyl isomerization of a ligand substituent.

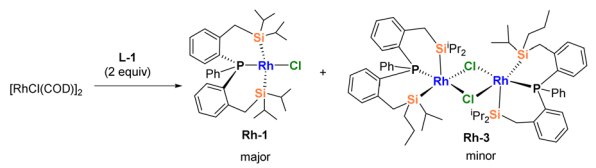

Scheme 2 The observed reactivity of [RhCl(COD)]$_2$ and **L-1** giving rise to complexes **Rh-1** and **Rh-3**.

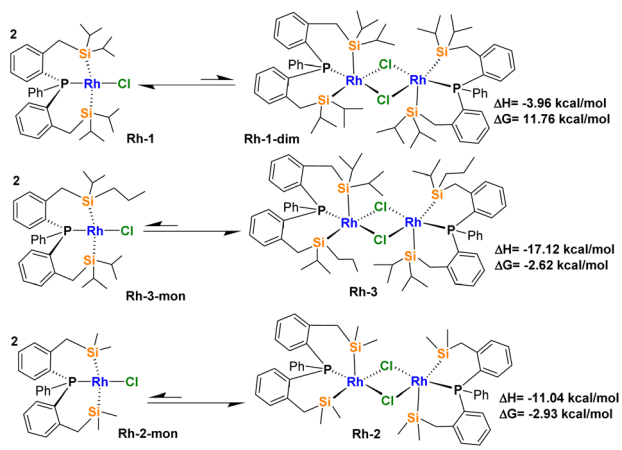

Scheme 3 The monomer/dimer equilibria upon variation of the substituents on Si in (κ^3-*Si*,*Si*,*P*)RhCl complexes and the calculated energetic parameters (at the ωB97XD/BS2//BS1 level of theory).

Results and discussion

Isolation of [(μ-Cl)Rh-(κ^3(*P*,*Si*,*Si*)PhP(*o*-$C_6H_4CH_2Si^iPr_2$)(*o*-$C_6H_4CH_2Si^iPr^nPr$)]$_2$ (Rh-3)

We previously reported the synthesis of complex **Rh-1**, isolated in 73% yield from the reaction of **L-1** and [RhCl(COD)]$_2$ in a 2 : 1 molar ratio in toluene. We have now identified complex **Rh-3** as a minor species in the same synthesis. Complex **Rh-3** was isolated as yellow crystals in 13–15% yield. The X-ray structure shows the formation of a dimeric structure with a notable feature. Out of the four substituents on the two Si atoms per coordinated ligand, a single isopropyl substituent has been isomerized to *n*-propyl. The highly symmetric structure shows a dimeric compound bridged by two chlorides. A square pyramidal geometry around each rhodium atom is generated from the coordination of the modified ligand in a facial mode (Fig. 1). The structural parameters are very close to those reported for complex **Rh-2**, with methyl substituents on Si. Notably, the Si1–Rh–Si2 angle at 96.95(3)° is almost identical to that in **Rh-2** at 96.92(3)°.[23] Other parameters such as the Rh–Si bond lengths here at 2.3147(9) Å and 2.3064(0) Å are close to those in **Rh-2** at 2.2960(6) and 2.2825(6) Å and **Rh-1** at 2.294(2) and 2.293(2) Å. The presence of an *n*-propyl substituent was further corroborated in solution by ^{13}C DEPT NMR experiments of the crystals, where two new methylene signals are observed at δ 20.88 and 18.84 ppm. The $^{31}P\{^1H\}$ and DEPT $^{29}Si\{^1H\}$ NMR signals are observed slightly upfield to those of complex **Rh-1** at δ 25.0 (d, J_{PRh} = 140 Hz) and 65.7 (dd, J_{Si-Rh} = 37.0, J_{Si-P} = 12.7 Hz) ppm, respectively.

The isomerization of alkanes is a fundamental reaction with industrial relevance. For example, the isomerization of linear alkanes is used in the production of gasolines with high octane values[30] and, the acid or bifunctional metal-acid catalyzed isomerization of cyclohexane is of interest in the reduction of benzene.[30] The isomerization of alkyl metal complexes has been amply studied as has the equilibria between isomeric alkyl-metal complexes where the linear alkyl group is often favored.[31] For example, hydrozirconation of isomers of octene leads to *n*-octylzirconium as the sole product. However, to the best of our knowledge, no other examples of alkyl isomerization of a ligand substituent have been reported to date. Yet, reversible and irreversible Si–C bond formation/cleavage has been well documented at various pincer complexes PSiP-M (PSiP = MeSi(*o*-C_6H_4-$PR_2)_2$, Chart 1). Indeed, methyl, ethyl, prenyl, and phenyl migration of a substituent on Si has been observed in Ni and Pd pincer motifs. In pincer PSiP-M-Me (M = Ni, Pd, Chart 1), Turculet and coworkers proposed the intermediacy of a 14-electron di-coordinated Pd or Ni(0) species, which would undergo Si–C(sp^2) oxidative addition to the ligand rearranged product, which featured a four-member

 This journal is © The Royal Society of Chemistry 2023

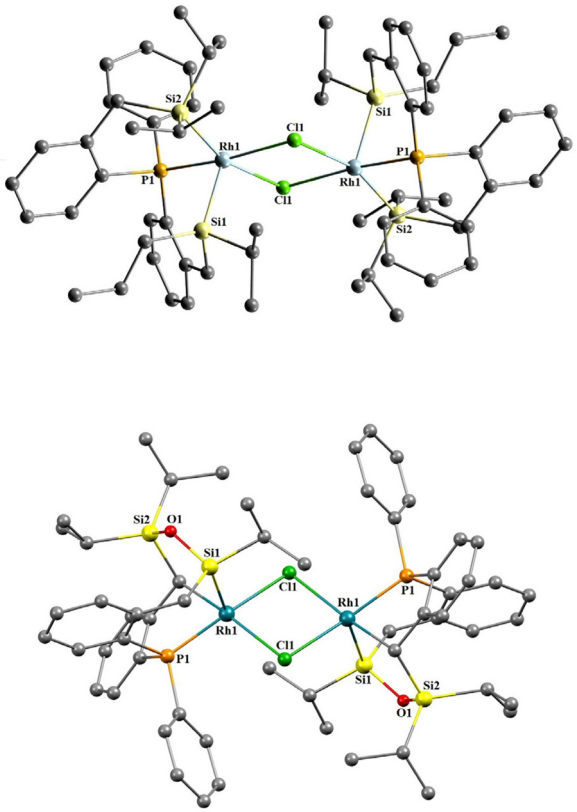

Fig. 1 From top to bottom, X ray diffraction structures of complexes **Rh-3** and **Rh-4**. The main structural parameters in Å and angles (°) are as follows: **Rh-3**: Rh1–Cl1 2.4217(10), Rh1–P1 2.2088(10), Rh1–Si1 2.3064(9), Rh1–Si2 2.3147(9), P1–Rh1–Cl1 172.308(17), Si1–Rh1–Cl1 102.23(2), Cl1–Rh1–Cl1#1 81.95(2), P1–Rh1–Si1 85.31(2), Si1–Rh–Si2 96.95(3); **Rh-4**: Rh1–Cl1 2.4167(15), Rh1–P1 2.2087(14), Rh1–Si1 2.2663(18), Si1–O1 1.649(4), Si2–O1 1.663(3), P1–Rh1–Cl1 97.46(5), Si1–Rh1–Cl1 97.68(6), Rh1–Cl1–Rh1 93.56(5), Si1–O1–Si2 122.6(2).

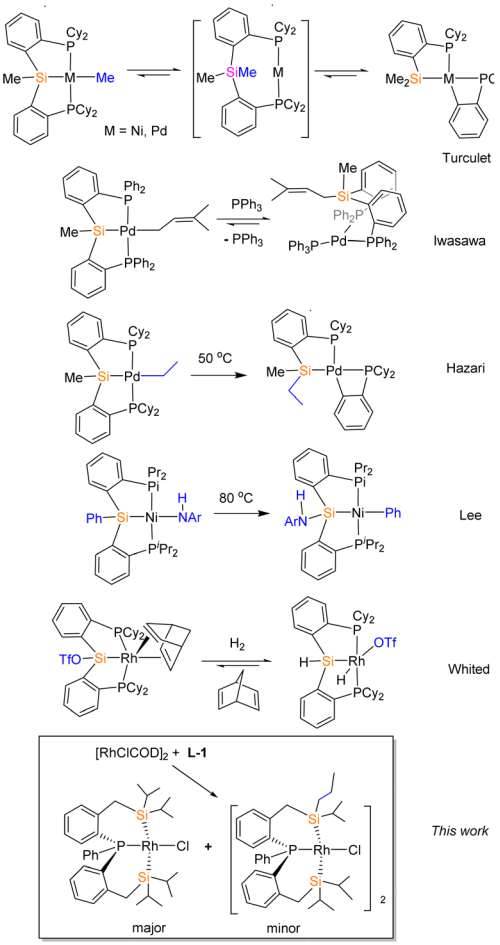

Chart 1 The reported examples of reversible substituent exchange in pincer PSiP complexes: alkyl, allyl, Ph, NHAr and OTf mentioned in the text. In this work, reversible isopropyl migration to Rh results in the isomerization of a single substituent on Si from the SiPSi pincer-like motif.

metallacycle.[25] The facile Si–C(sp^3) and Si–C(sp^2) formation reactions account for the reversibility of the processes/formation reactions account for the reversibility of the processes that occur at rates in the timescale of the NMR experiments.[26,32] Hazari and coworkers observed similar reactivity from the β-hydride elimination Pd complex to the rearranged products in the presence of ethylene (Chart 1).[27] Takaya, Iwasawa, and coworkers were able to isolate a tricoordinate Pd complex, where a new Si–C(sp^3) bond is reversibly formed replacing the Pd–Si bond.[28,29] Other notable examples of reversible ligand substituent exchange provided also by the PSiP ligand framework suggest a M–Si cooperation in catalytic and stoichiometric processes such as in the reversible exchange of triflate between Si and Rh in Rh(PSiP) systems by Whited and coworkers, which allows for the addition of hydrogen across the Rh–Si bond.[33] Similarly, the exchange of amide and phenyl moieties in Ni(PSiP) by Lee and coworkers was found to facilitate CO_2 functionalization (Chart 1).[34]

Additionally, the presence of adventitious water in the solvent system during the reaction of $[RhCl(COD)]_2$ and **L-1** led to the formation of **Rh-4**, which crystallizes as light yellow crystals (Scheme 2). The crystals were isolated in very small yield, 5%, and characterized in the solid state by X-ray diffraction and in solution by spectroscopic means. The solution $^{31}P\{^1H\}$ NMR spectrum of **Rh-4** shows a doublet signal at 49.0 ppm (d, J_{PRh} = 164.0 Hz). The X-ray diffraction structure (Fig. 1) discloses a symmetric dichloro-bridged dimetallic species with modified ligands. The coordination geometry around each Rh center can be described as distorted square pyramidal. Each pentacoordinated Rh(III) metal center is bound to the phosphorus atom, a benzylic carbon and only one silicon atom of the ligand. The new Rh–C bonds result from intramolecular benzylic C–H activation of the formerly methylene carbon. The Si atom bound to Rh bears only one isopropyl substituent whereas the other silicon atom, alfa to the cyclometallated C, no longer binds to Rh but instead to O, forming part of a Si–O–Si motif. The bond lengths and angles are within the expected ranges of other siloxanes.[37–39] The formation of Si–O–Si complexes has been reported by several authors (Chart S1†). For example, oxidation of the Pt disilene complex

$[(PR_3)_2Pt\text{-}\eta^2(Mes_2Si{=}SiMes_2)]$[40] by West and coworkers, and dehydrogenative condensation on $[(dmpe)Pt(SiHPh_2)_2]$ upon reaction with water by Osakada and coworkers,[41] rendered four-membered Si–O–Si platinacycle units. Ozerov and coworkers reported Si–O–Si motifs bridging two Pt units from the reaction of adventitious water with three-coordinate cationic Pt-PSiP,[42] in a variation of Milstein's saturated Cl–Pt–PSiP system, in which the rearrangement of a pincer silanol Pt complex in the presence of water and a non-nucleophilic base led to a binuclear complex bearing a Si–O–Si–O motif bridging two Pt centers.[43] Adventitious water also reacts with a terminal silylene[44] or σ(Si–H) complexes[23] forming bimetallic Si–O–Si bridges spanning two Ir or Rh centers as reported by Tilley and coworkers (Chart S1†).

Computations on the monomer–dimer equilibrium in Rh-1 and Rh-2 complexes

We previously suggested the existence of a 14-electron monomer/16-electron dimer equilibrium to explain the reactivity of the related **Ir-2** complex, with methyl substituents on the Si atoms, which gives rise to monometallic products upon reaction with two-electron donors.[24] We now computed the DFT structures of complexes **Rh-1**, **Rh-2** and **Rh-3-mon** at ωB97XD/BS2//BS1 level theory. We calculated the thermodynamic parameters ΔH and ΔG for a monomer–dimer equilibria hypothetically established in the three Rh complexes (Scheme 3). The calculated Gibbs free energies were determined as −2.93 and −2.62 kcal mol^{-1} for **Rh-2** and **Rh-3**, respectively. These favorable and similar values are in agreement with the observed dimerization of the methyl substituted complex **Rh-2** and the *n*-propyl/isopropyl complex **Rh-3**. In contrast, the dimerization process is unfavorable by 11.8 kcal mol^{-1} for the all-isopropyl substituted **Rh-1** complex. Thus, the modification of only one of the substituents on Si in **Rh-3** considerably changes the energetics of the system. These findings are relevant for the understanding of important catalytic species. For example, the catalytic activity of 16-electron chloro bisphosphine Rh(I) dimers of the type $[Rh(PP)(\mu\text{-}Cl)]_2$, where PP is a diphosphine, such as dppe, dppp, diphos, JohnPhos, *etc.*,[10,15,35] is proposed to be triggered by the formation of the 14-electron unsaturated monomers. Experimental observation of such phenomena is of course limited given the rapid dimer–monomer equilibrium resulting often in identical NMR chemical shifts; however, techniques such as DOSY NMR and kinetic determinations complement the computational studies.[10,36]

Experimental findings on the mechanism of formation of Rh-3

In order to rule out the formation of **Rh-3** from **Rh-1**, pure samples of **Rh-1** under different conditions of solvent (benzene-d_6, toluene-d_8 and $CDCl_3$) and temperature (room temperature and 50 °C) were monitored by NMR spectroscopy. We found no evidence of the conversion of **Rh-1** to **Rh-3** even after one month at 50 °C. Given that we previously reported the exchange of the Cl ligand in **Rh-1** by other halogens upon addition of the corresponding Na or Ag salts,[17] varying amounts of KCl or NaCl salts were added to the **Rh-1** solutions to favor a possible dissociation of the coordinated Cl in **Rh-1**, which could trigger isopropyl migration and isomerization. However, no changes were noticed under those conditions either. These observations allow us to conclude that **Rh-3** is not formed from **Rh-1** but it is likely generated during the metalation process from $[RhCl(COD)]_2$ and **L-1**. Finally, the reaction of $[RhCl(COD)]_2$ with **L-1** led to slightly different ratios of **Rh-1** : **Rh-3** (Table 1) when performed in benzene or toluene. However, the reaction in other solvents such as pentane, dichloromethane, acetonitrile and THF did not lead to the experimental observation of **Rh-3**.

Computations on the mechanism for the observed isomerization of iso-propyl to *n*-propyl to form complex Rh-3

We explored the formation of complex **Rh-3** from two potential pathways: (1) directly in the metalation reaction from $[RhCl(COD)]_2$ and **L-1** and (2) from a rearrangement proceeding from **Rh-1**. The value of $\Delta\Delta G^\circ$ between **Rh-1** and the *n*-propyl isomer, **Rh-3-mon**, is very small ($\Delta\Delta G^\circ$ = −1.9 kcal mol^{-1}). Since experimentally, only a small amount of **Rh-3** is observed, this result suggests that the isomer selectivity is controlled kinetically rather than thermodynamically. Based on the experimental findings, it is probable that **Rh-3** is directly produced through metalation. Using computational tools, we propose a mechanism consisting of two main parts. First, the formation of intermediate **Rh-8** occurs during metalation (Fig. 2). From this intermediate, two competitive pathways arise, leading to the formation of **Rh-1** and its isomer, **Rh-3-mon** (Fig. 3).

In the first part (Fig. 2), the oxidative addition of a single Si–H bond of **L-1** to the monomeric **RhCl(COD)** produces **Rh-5** species, which is slightly endergonic (ΔG° = 3.8 kcal mol^{-1}). Subsequent steps involve hydride migratory insertion (hydride M/I), σ-bond metathesis, and reductive elimination (RE), as shown in Fig. 2, which represents the energetically favorable path. The order of these steps can vary, resulting in different pathways to **Rh-8** (details in Fig. S8†). In **TS5–6** ($\Delta^\ddagger G^\circ$ = 27.8 kcal mol^{-1}), in addition to the transfer of the hydride to the COD ligand, the hydrogen atom from the agostic Si–H

Table 1 Calculated ratios of the **Rh-1** : **Rh-3** monomer by DFT computations and comparisons with experimental data from $^{31}P\{^1H\}$ spectroscopy from *in situ* metalations

Method	**Rh-1**/**Rh-3-mon** ratio	$\Delta\Delta^\ddagger G^\circ$ (kcal mol^{-1})
Experiment in benzene	85 : 15[a]	1.0
SMD(benzene)//ωB97XD/BS1	83 : 17	0.94
Experiment in toluene	77 : 23[a,b]	0.72[b]
SMD(toluene)//ωB97XD/BS1	79 : 21	0.78

[a] These approximate ratios were calculated by integration of the signals in the $^{31}P\{^1H\}$ spectra considering one P nuclei per **Rh-3** as a monomer. The reactions were performed *in situ* in NMR tubes in the corresponding solvents. [b] The integrations of the closely spaced signals in the $^{31}P\{^1H\}$ spectrum were approximated to the given values by deconvolution of the signals.

This journal is © The Royal Society of Chemistry 2023

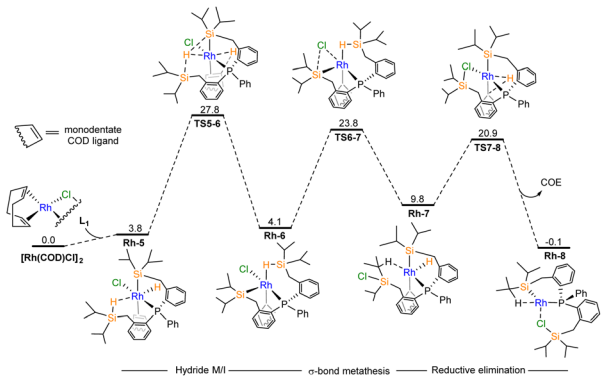

Fig. 2 Gibbs free energy diagram (kcal mol^{-1}) from DFT computations at SMD(benzene)//ωB97XD/BS1 level theory in the formation of the **Rh-8** intermediate. Hydride M/I = hydride migratory insertion.

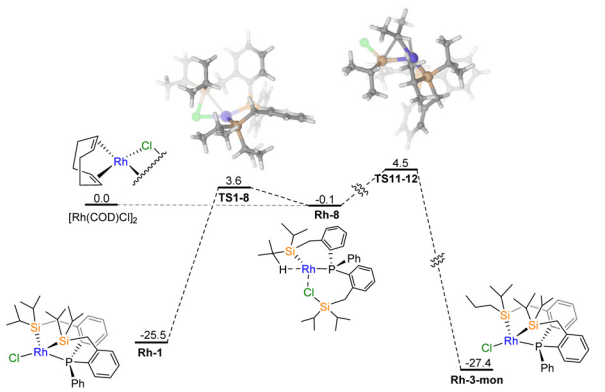

Fig. 3 Simplified Gibbs free energy diagram (kcal mol^{-1}) of the kinetic control of **Rh-1** and isomer **Rh-3-mon** from DFT computations at SMD (benzene)//ωB97XD/BS1 level theory.

bond also moves to another silicon atom, exemplifying the hydride relay properties. The formation of Si–Cl bond *via* **TS6–7** ($\Delta^{\ddagger}G^{\circ}$ = 23.8 kcal mol^{-1}) leads to the oxidative addition of the remaining Si–H bond. Consequently, the term "σ-bond metathesis" is suitable to describe the transformation of **Rh-6** to **Rh-7**, where Rh(III) retains its oxidation state. The C–H RE step **TS7–8** ($\Delta^{\ddagger}G^{\circ}$ = 20.9 kcal mol^{-1}) transfers another hydrogen to the COD ligand, converting it to COE, observed experimentally by NMR, as the side product of the metalation process and resulting in the formation of the **Rh-8** complex.

In the subsequent process, starting from the **Rh-8** species, either **Rh-1** or **Rh-3-mon** can be formed as proposed in Fig. 3. **Rh-1** can be directly produced through Si–Cl bond oxidative addition steps in **TS1–8** ($\Delta^{\ddagger}G^{\circ}$ = 3.6 kcal mol^{-1}), while multiple steps are required to generate the **Rh-3-mon** complex (for detailed information, refer to Fig. S10†). It is important to note that there are several intermediate steps between **Rh-8** and **Rh-3-mon**; however, for the purpose of clarity and simplicity, only the highest energy transition state **TS11–12** is depicted in Fig. 3. The isomer selectivity in this case can be understood using the Curtin–Hammett principle. The predominance of **Rh-1** over **Rh-3-mon** is primarily attributed to the lower energy requirement of the kinetic path, which is 3.6 kcal mol^{-1} compared to 4.5 kcal mol^{-1}. The energy gap value between these two transition states **TS1–8** and **TS11–12** is small, with $\Delta\Delta^{\ddagger}G^{\circ}$ = 0.9 kcal mol^{-1}, and it poses a general challenge to computational studies. However, the calculation at SMD(benzene)//ωB97XD/BS1 level theory fortuitously gives a value very close (0.94) to the experimentally determined value of 1.0 kcal mol^{-1} (Table 1). It is important to note that while the proposed mechanism in Fig. 2 and 3 provides insights into the formation of both isomers, DFT calculations should not be solely relied upon for quantifying the ratio.

Computed selectivity values **Rh-1 : Rh-3-mon** in benzene and toluene show small changes in the product selectivity. Indeed, the computed benzene and toluene ratios are very close to those obtained experimentally (Table 1). As stated before, **Rh-3** was not detected experimentally when the reaction was carried out in pentane. Furthermore, the proposed mechanism is no longer valid in polar solvents such as tetrahydrofuran or dichloromethane, which can also act as ligands and lead to a significant change in the nature of the process, as corroborated experimentally where no **Rh-3** is observed.

Overall, the direct formation of **Rh-3** from [RhCl(COD)]$_2$ exhibits an apparent kinetic free energy of activation of $\Delta\Delta^{\ddagger}G^{\circ}$ = 25.3 kcal mol^{-1}. The free energy of activation for the formation of **Rh-3** from **Rh-1** is higher, with an apparent free energy of activation of $\Delta\Delta^{\ddagger}G^{\circ}$ = 28.4 kcal mol^{-1} (energy gap between **Rh-1** and **TS11–12**). This result is consistent with the experimental findings and demonstrates that the direct pathway is energetically favorable. Furthermore, several other pathways including through a silylene intermediate, σ-bond metathesis, and reductive elimination were also considered but have unfavorable energies (Fig. S9†).

In our case, stoichiometric addition of water to either **Rh-1** or **Rh-3** does not lead to the formation of **Rh-4** but instead, other unidentified products are generated. We thus propose that complex **Rh-4** is also formed during the metalation process from the reaction of one of the intermediate species with adventitious water.

Conclusions

In conclusion, alkyl isomerization at the silicon ligand **L-1** yields the 16-electron dimer **Rh-3** in *ca.* 13–15% isolated yield where one of the two silicon atoms bears an *n*-propyl substituent. The dimerization of the mixed *n*-propyl/isopropyl **Rh-3-mon** to **Rh-3** (the dimer) is energetically favored as is the dimerization of the methyl analogue, **Rh-2-mon** to **Rh-2** (the dimer). In contrast, **Rh-1** with four isopropyl substituents on the two silicon atoms does not undergo dimerization. Once a dimeric species is formed, isopropyl migration to Rh is no longer possible accounting for the lack of detection of doubly or further isomerized products. Dimer **Rh-3** is formed during the metalation process from [RhCl(COD)]$_2$ through an alternative pathway to that of the major formation of **Rh-1**. The revers-

ible transfer of an isopropyl substituent to Rh allows for isomerization at the metal center followed by migration back to the silicon atom. This work is in line with the proposed cooperative partnership between Rh and Si which could allow for different reactivity at complexes bearing this type of ligand.

Experimental section

General considerations

Experiments were performed under an argon atmosphere using standard Schlenk methods or in an MBraun glove box unless stated otherwise. Laboratory solvents were dried and purified over MBraun column systems. Benzene-d_6 was passed through a Pasteur pipette containing molecular sieves and then degassed *via* three freeze–pump–thaw cycles and stored over molecular sieves. The other reagents were purchased from Sigma Aldrich and used as received. Nuclear magnetic resonance (NMR) experiments were performed on Bruker Avance 300, 500 and 600 spectrometers. All chemical shifts (δ) for ^{1}H, ^{29}Si and ^{13}C are relative to TMS and are reported in parts per million (ppm).

[(μ-Cl)Rh-(κ^3(*P*,*Si*,*Si*)PhP(*o*-$C_6H_4CH_2Si^iPr_2$)(*o*-$C_6H_4CH_2Si^iPr^nPr$)]$_2$ (Rh-3)

In a Schlenk flask, 47 mg (0.097 mmol) of [RhCl(COD)]$_2$ and 100 mg of **L-1** (0.19 mmol) were dissolved together in 2 mL of freshly dry toluene. The resulting orange solution was left stirring for 3 hours at room temperature. Subsequently, the solution was concentrated under vacuum and crystals of **Rh-1** were removed. Then, the mother liquor was dried and redissolved in pentane. Orange crystals of complex **Rh-3** were grown from this pentane solution. ^{1}H NMR (600 MHz, C_6D_6, 298 K): δ 7.04–6.84 (m, 21H, CH_{arom}), 6.77–6.71 (m, 5H, CH_{arom}), 2.30–2.23 (m, 4H, CH_2), 2.14 (dd, J_{HH} = 14.6, J_{HP} = 2.9 Hz, 2H, CH_2), 2.03 (d, J_{HH} = 14.4 Hz, 2H, CH_2), 2.01–1.86 (m, 2H, CH-^{i}Pr), 1.77–1.63 (m, 4H, CH-^{i}Pr), 1.61 (d, J_{HH} = 7.2 Hz, 6H, CH_3-^{i}Pr), 1.58–1.51 (m, 4H, CH_2-propyl), 1.32 (ddd, J_{HH} = 14.6, J_{HH} = 12.7, J_{HP} = 3.9 Hz, 4H, CH_2-propyl, overlapped), 1.19 (d, J_{HH} = 7.5 Hz, 6H, CH_3-^{i}Pr), 1.13 (d, J_{HH} = 7.3 Hz, 6H, CH_3-^{i}Pr), 1.08 (d, J_{HH} = 7.4 Hz, 6H, CH_3-^{i}Pr), 1.01 (d, J_{HH} = 7.5 Hz, 6H, CH_3-^{i}Pr), 0.99–0.96 (overlapped signals: 12H, CH_3-^{i}Pr (6H) and CH_3-propyl (6H)). DEPT ^{13}C{^{1}H} NMR (150.9 MHz, C_6D_6): 24.02 (d, J_{CP} = 16.9 Hz, CH_2), 23.07 (d, J_{CP} = 18.3 Hz, CH_2), 21.94 (s, *C*H$_3$, ^{i}Pr), 20.88 (s, CH_2, *n*-propyl), 20.59 (s, CH, ^{i}Pr), 20.53 (s, CH, ^{i}Pr), 20.28 (s, CH_3, ^{i}Pr), 20.07 (s, CH_3, ^{i}Pr), 19.87 (s, CH_3, *n*-propyl), 19.20 (s, CH_3, ^{i}Pr), 18.84 (s, CH_2, *n*-propyl), 18.51 (s, CH_3, ^{i}Pr), 18.41 (s, CH_3, *n*-propyl). ^{31}P{^{1}H} NMR (202.46 MHz, C_6D_6): 31.5 (d, J_{PRh} = 145.7 Hz).

Observation of [μ-Cl-Rh{κ^3(*P*,*Si*,*C*)PPh(*o*-$C_6H_4CH_2Si^iPrO Si^iPr_2CH$-*o*-$C_6H_4$)}]$_2$ (Rh-4)

A reaction involving 47 mg (0.097 mmol) of [RhCl(COD)]$_2$ and 100 mg of **L-1** (0.19 mmol) in 2 mL of toluene (not rigorously dried) led to the isolation of orange crystals of **Rh-1**. The mother liquor was fully dried and redissolved in pentane, in an attempt to isolate crystals of **Rh-3**. However, after four weeks, a small amount of yellow crystals of complex **Rh-4** suitable for X-ray diffraction analysis were formed. Isolated yield 6 mg, 5%. **^{1}H NMR (500 MHz, C_6D_6, 298 K):** δ 7.48–7.37 (m, 5H, CH_{arom}), 7.13–6.97 (m, 31H, CH_{arom}), 2.58–2.24 (m, 4H, CH_2), 1.80 (sept, J_{HH} = 7.1 Hz, 4H, CH-^{i}Pr), 1.49 (d, J_{HH} = 7.6 Hz, 6H, CH_3-^{i}Pr), 1.41 (d, J_{HH} = 6.8 Hz, 6H, CH_3-^{i}Pr), 0.84 (d, J_{HH} = 7.5 Hz, 12H, CH_3-^{i}Pr), 0.60 (d, J_{HH} = 7.4 Hz, 6H, CH_3-^{i}Pr), 0.38 (d, J_{HH} = 7.5 Hz, 6H, CH_3-^{i}Pr), 0.10–0.02 (m, 2H, CH-^{i}Pr), ppm. **^{31}P{^{1}H} NMR (202.46 MHz, C_6D_6):** 49.04 (d, J_{PRh} = 164.0 Hz) ppm.

Conflicts of interest

There are no conflicts to declare.

Acknowledgements

This work was financially supported by the NSF Division of Chemistry projects, CHE 2102689 and CHE 2102552. The Mississippi Center for Supercomputing Research is acknowledged for computing resources. We would like to thank Professor Bill Jones (Rochester) for an exciting discussion.

References

1 R. Singh, V. D. Goyal, A. Kumar, N. S. Sabharwal and R. D. Makde, Crystal structures and biochemical analyses of intermediate cleavage peptidase: Role of dynamics in enzymatic function, *FEBS Lett.*, 2019, **593**, 443–454.

2 A. J. Jackson-Fisher, S. Burma, M. Portnoy, L. A. Schneeweis, R. A. Coleman, M. Mitra, C. Chitikila and B. F. Pugh, Dimer dissociation and thermosensitivity kinetics of the *Saccharomyces cerevisiae* and human TATA binding proteins, *Biochemistry*, 1999, **38**, 11340–11348.

3 D. Madern, C. Ebel, M. Mevarech, S. B. Richard, C. Pfister and G. Zaccai, Insights into the molecular relationships between malate and lactate dehydrogenases: Structural and biochemical properties of monomeric and dimeric intermediates of a mutant of tetrameric L-[LDH-like] malate dehydrogenase from the halophilic archaeon *Haloarcula marismortui*, *Biochemistry*, 2000, **39**, 1001–1010.

4 D. Srivastava, S. Nandi and M. Dey, Mechanistic and structural insights into cysteine-mediated inhibition of pyruvate kinase muscle isoform 2, *Biochemistry*, 2019, **58**, 3669–3682.

5 M. Fox, H. R. Mott and D. Owen, Class IA PI3K regulatory subunits: p110-independent roles and structures, *Biochem. Soc. Trans.*, 2020, **48**, 1397–1417.

6 H. Blanchard, K. Bum-Erdene, M. H. Bohari and X. Yu, Galectin-1 inhibitors and their potential therapeutic applications: A patent review, *Expert Opin. Ther. Pat.*, 2016, **26**, 537–554.

 This journal is © The Royal Society of Chemistry 2023

7 B. K. Gilsbach, M. Eckert, C. J. Gloeckner and C. J. Gloeckner, Regulation of LRRK2: Insights from structural and biochemical analysis, *Biol. Chem.*, 2018, **399**, 637–642.

8 M. Urscher, R. Alisch and M. Deponte, The glyoxalase system of malaria parasites—Implications for cell biology and general glyoxalase research, *Semin. Cell Dev. Biol.*, 2011, **22**, 262–270.

9 O. Delelis and E. Deprez, Interplay between DNA-binding/catalytic functions and oligomerization of retroviral integrases studied by a combination of time-resolved fluorescence anisotropy, fluorescence correlation spectroscopy and resonance energy transfer, *Rev. Fluoresc.*, 2016, **8**, 301–336.

10 A. Mannu, M. Ferro, S. Moeller and D. Heller, Monomerisation of $[Rh_2(1,3\text{-bis-(diphenylphosphino)-propane})_2(\mu_2\text{-Cl})_2]$ detected by pulsed gradient spin echo spectroscopy and ^{31}P NMR monitoring of metathesis experiments, *J. Chem. Res.*, 2018, **42**, 402–404.

11 E. Alberico, S. Moller, M. Horstmann, H.-J. Drexler and D. Heller, Activation, deactivation and reversibility phenomena in homogeneous catalysis: A showcase based on the chemistry of rhodium/phosphine catalysts, *Catalysts*, 2019, **9**, 582.

12 G. Makado, T. Morimoto, Y. Sugimoto, K. Tsutsumi, N. Kagawa and K. Kakiuchi, Highly linear-selective hydroformylation of 1-alkenes using formaldehyde as a syngas substitute, *Adv. Synth. Catal.*, 2010, **352**, 299–304.

13 T. Furusawa, T. Morimoto, Y. Nishiyama, H. Tanimoto and K. Kakiuchi, Rh^I-Catalyzed intramolecular carbonylative C-H/C-I coupling of 2-iodobiphenyls using furfural as a carbonyl source, *Chem. – Asian J.*, 2016, **11**, 2312–2315.

14 M. Pareek and R. B. Sunoj, Energetics of dynamic kinetic asymmetric transformation in Suzuki–Miyaura coupling, *ACS Catal.*, 2020, **10**, 4349–4360.

15 U. Gellrich, A. Meißner, A. Steffani, M. Kähny, H.-J. Drexler, D. Heller, D. A. Plattner and B. Breit, Mechanistic investigations of the rhodium catalyzed propargylic CH activation, *J. Am. Chem. Soc.*, 2014, **136**, 1097–1104.

16 P. Koschker, M. Kähny and B. Breit, Enantioselective redox-neutral Rh-catalyzed coupling of terminal alkynes with carboxylic acids toward branched allylic esters, *J. Am. Chem. Soc.*, 2015, **137**, 3131–3137.

17 N. S. Abeynayake, J. Zamora-Moreno, S. Gorla, B. Donnadieu, M. A. Munoz-Hernandez and V. Montiel-Palma, 14-Electron Rh and Ir silylphosphine complexes and their catalytic activity in alkene functionalization with hydrosilanes, *Dalton Trans.*, 2021, **50**, 11783–11792.

18 M. V. Corona-González, J. Zamora-Moreno, M. A. Muñoz-Hernández, L. Vendier, S. Sabo-Etienne and V. Montiel-Palma, Exploiting the versatility of phosphinobenzylsilanes for the stabilization of 14-electron rhodium(III) and iridium (III) complexes, *Eur. J. Inorg. Chem.*, 2019, **2019**, 1854–1858.

19 S. Gorla, M. L. Díaz-Ramírez, N. S. Abeynayake, D. M. Kaphan, D. R. Williams, V. Martis, H. A. Lara-García, B. Donnadieu, N. Lopez, I. A. Ibarra and V. Montiel-Palma, Functionalized NU-1000 with an iridium organometallic fragment: SO_2 capture enhancement, *ACS Appl. Mater. Interfaces*, 2020, **12**, 41758–41764.

20 M. A. Esteruelas, I. Fernández, A. Martínez, M. Oliván, E. Oñate and A. Vélez, Iridium-promoted B–B bond activation: Preparation and X-ray diffraction analysis of a mer-Tris(boryl) complex, *Inorg. Chem.*, 2019, **58**, 4712–4717.

21 J. Zhu, Z. Lin and T. B. Marder, Trans influence of boryl ligands and comparison with C, Si, and Sn ligands, *Inorg. Chem.*, 2005, **44**, 9384–9390.

22 H. Kameo, S. Ishii and H. Nakazawa, Synthesis of iridium complexes bearing $\{o\text{-}(Ph_2P)C_6H_4\}_3E$ type (E = Si, Ge, and Sn) ligand and evaluation of electron donating ability of group 14 elements E, *Dalton Trans.*, 2012, **41**, 8290–8296.

23 M. V. Corona-Gonzalez, J. Zamora-Moreno, C. A. Cuevas-Chavez, E. Rufino-Felipe, E. Mothes-Martin, Y. Coppel, M. A. Munoz-Hernandez, L. Vendier, M. Flores-Alamo, M. Grellier, S. Sabo-Etienne and V. Montiel-Palma, A family of rhodium and iridium complexes with semirigid benzylsilyl phosphines: From bidentate to tetradentate coordination modes, *Dalton Trans.*, 2017, **46**, 8827–8838.

24 C. A. Cuevas-Chávez, L. Vendier, S. Sabo-Etienne and V. Montiel-Palma, Iridium complexes featuring a tridentate SiPSi ligand: From dimeric to monomeric 14, 16 or 18-electron species, *Dalton Trans.*, 2019, **48**, 14010–14018.

25 S. J. Mitton, R. McDonald and L. Turculet, Nickel and palladium silyl pincer complexes: Unusual structural rearrangements that involve reversible Si–C(sp^3) and Si–C(sp^2) bond activation, *Angew. Chem., Int. Ed.*, 2009, **48**, 8568–8571.

26 S. J. Mitton, R. McDonald and L. Turculet, Facile intramolecular silicon–carbon bond activation at Pt0 and PtII centers, *Polyhedron*, 2013, **52**, 750–754.

27 H.-W. Suh, L. M. Guard and N. Hazari, A mechanistic study of allene carboxylation with CO_2 resulting in the development of a Pd(ii) pincer complex for the catalytic hydroboration of CO_2, *Chem. Sci.*, 2014, **5**, 3859–3872.

28 J. Takaya and N. Iwasawa, Hydrocarboxylation of allenes with CO_2 catalyzed by silyl pincer-type palladium complex, *J. Am. Chem. Soc.*, 2008, **130**, 15254–15255.

29 J. Takaya and N. Iwasawa, Bis(*o*-phosphinophenyl)silane as a scaffold for dynamic behavior of H–Si and C–Si bonds with palladium(0), *Organometallics*, 2009, **28**, 6636–6638.

30 A. Alazman, D. Belic, A. Alotaibi, E. F. Kozhevnikova and I. V. Kozhevnikov, Isomerization of cyclohexane over bifunctional Pt-, Au-, and PtAu-heteropoly acid catalysts, *ACS Catal.*, 2019, **9**, 5063–5073.

31 J. N. Harvey, Electronic effects on the stability of isomeric alkyl transition metal compounds, *Organometallics*, 2001, **20**, 4887–4895.

32 E. Sola, in *Pincer compounds: Chemistry and applications*, ed. D. Morales-Morales, Elsevier, Amsterdam, Netherlands, 2018, pp. 401–413.

33 M. T. Whited, A. M. Deetz, T. M. Donnell and D. E. Janzen, Examining the role of Rh/Si cooperation in alkene hydrogenation by a pincer-type $[P_2Si]Rh$ complex, *Dalton Trans.*, 2016, **45**, 9758–9761.

34 J. Kim, Y.-E. Kim, K. Park and Y. Lee, A silyl-nickel moiety as a metal–ligand cooperative site, *Inorg. Chem.*, 2019, **58**, 11534–11545.
35 S. M. Jackson, C. E. Hughes, S. Monfette and L. Rosenberg, Structural criteria for the activity of rhodium(I) phosphine complexes in the catalytic dehydrocoupling of di-n-hexylsilane, *Inorg. Chim. Acta*, 2006, **359**, 2966–2972.
36 S. Moller, N. Jannsen, J. Rueger, H.-J. Drexler, M. Horstmann, F. Bauer, B. Breit and D. Heller, Catalyst deactivation during rhodium complex-catalyzed propargylic C–H activation, *Chem. – Eur. J.*, 2021, **27**, 14034–14041.
37 J. Y. Corey, Reactions of hydrosilanes with transition metal complexes, *Chem. Rev.*, 2016, **116**, 11291–11435.
38 J. Y. Corey and J. Braddock-Wilking, Reactions of hydrosilanes with transition-metal complexes: Formation of stable transition-metal silyl compounds, *Chem. Rev.*, 1999, **99**, 175–292.
39 J. Y. Corey, Reactions of hydrosilanes with transition metal complexes and characterization of the products, *Chem. Rev.*, 2011, **111**, 863–1071.
40 E. K. Pham and R. West, Platinum .eta.2-disilene complexes: Syntheses, reactivity, and structures, *Organometallics*, 1990, **9**, 1517–1523.
41 H. Noda, K. Tanaka, M. Tanabe and K. Osakada, Cyclic platina(borasiloxane)s and platina(siloxane)s and their chemical properties, *Organometallics*, 2018, **37**, 22–29.
42 J. C. DeMott, W. Gu, B. J. McCulloch, D. E. Herbert, M. D. Goshert, J. R. Walensky, J. Zhou and O. V. Ozerov, Silyl–silylene interplay in cationic PSiP pincer complexes of platinum, *Organometallics*, 2015, **34**, 3930–3933.
43 E. E. Korshin, G. Leitus, L. J. W. Shimon, L. Konstantinovski and D. Milstein, Silanol-based pincer Pt(II) complexes: Synthesis, structure, and unusual reactivity, *Inorg. Chem.*, 2008, **47**, 7177–7189.
44 J. D. Feldman, J. C. Peters and T. D. Tilley, Activations of silanes with $[PhB(CH_2PPh_2)_3]Ir(H)(\eta_3\text{-}C_8H_{13})$. Formation of iridium silylene complexes via the extrusion of silylenes from secondary silanes R_2SiH_2, *Organometallics*, 2002, **21**, 4065–4075.

This journal is © The Royal Society of Chemistry 2023